Effects of Alpha–Proton Differential Flow on Proton Temperature Anisotropy Instabilities in the Solar Wind: *Wind* Observations

G. Q. Zhao[1,2] , H. Li[3,4] , H. Q. Feng[1] , D. J. Wu[5] , H. B. Li[1], and A. Zhao[1]
[1] Institute of Space Physics, Luoyang Normal University, Luoyang, People's Republic of China
[2] Henan Key Laboratory of Electromagnetic Transformation and Detection, Luoyang, People's Republic of China
[3] State Key Laboratory of Space Weather, National Space Science Center, CAS, Beijing, People's Republic of China
[4] University of Chinese Academy of Sciences, Beijing, People's Republic of China
[5] Purple Mountain Observatory, CAS, Nanjing, People's Republic of China

Abstract

Plasma kinetic waves and alpha–proton differential flow are two important subjects on the topic of solar wind evolution. Based on the *Wind* data during 2005–2015, this paper reports that the occurrence of electromagnetic cyclotron waves (ECWs) near the proton cyclotron frequency significantly depends on the direction of alpha–proton differential flow V_d. As V_d rotates from the anti-Sunward direction to the Sunward direction, the occurrence rate of ECWs as well as the percentage of left-handed (LH) polarized ECWs decreases considerably. In particular, it is shown that the dominant polarization changes from LH polarization to right-handed polarization during the rotation. The investigation on proton and alpha particle parameters ordered by the direction of V_d further illustrates that large kinetic energies of alpha–proton differential flow correspond to high occurrence rates of ECWs. These results are consistent with theoretical predictions for effects of alpha–proton differential flow on proton temperature anisotropy instabilities.

Key words: instabilities – interplanetary medium – solar wind – waves

1. Introduction

The investigation of kinetic waves as well as kinetic instabilities is believed to be inherently important for the topic of energizing particles and/or modifying their velocity distributions in a collisionless plasma (e.g., Hollweg 1975; Marsch 2006). In particular, electromagnetic cyclotron waves (ECWs) near the proton cyclotron frequency are of particular interest; theoretical studies show that they can efficiently contribute their energy to particles or absorb energy from the particles through wave–particle resonant interactions (Marsch et al. 1982a; Hu & Rifai Habbal 1999; He et al. 2015, 2018; Woodham et al. 2018). They have been extensively studied in various space environments, such as planetary magnetosphere (e.g., Russell & Blancocano 2007; Rodríguez-Martínez et al. 2010), magnetosheath (e.g., Schwartz et al. 1996; Soucek et al. 2015), and terrestrial foreshock regions (e.g., Smith et al. 1985; Wong et al. 1991). In the case of the solar wind, research on ECWs has obtained a lot of interest in recent years (e.g., Jian et al. 2009, 2010, 2014; Boardsen et al. 2015; Gary et al. 2016; Xiang et al. 2018a, 2018b; Li et al. 2019; Zhao et al. 2019). According to observations, in the case of parallel propagation, and at scales close to the proton gyro-frequency, a noticeable result is that left-handed (LH) polarized ECWs are almost always the dominant waves in the solar wind (e.g., Boardsen et al. 2015; Zhao et al. 2018). The polarization is described in the spacecraft frame and with respect to the direction of the background magnetic field throughout the paper except where noted. Theoretically, two kinetic instabilities driven by proton temperature anisotropies can contribute to the generation of the ECWs consisting of LH proton cyclotron waves and right-handed (RH) magnetosonic waves in the plasma frame (Gary et al. 1976; Gary 1993, 2015; Kasper et al. 2002; Marsch et al. 2004; Hellinger et al. 2006; Omidi et al. 2014; Yoon 2017). Proton cyclotron instability can be excited to produce cyclotron waves in a plasma with proton perpendicular temperature ($T_\perp$) larger than the parallel temperature ($T_\parallel$), while parallel firehose

instability may arise to generate magnetosonic waves in a plasma with a converse temperature anisotropy ($T_\perp < T_\parallel$).

On the other hand, the phenomena of differential flow between alpha particles and protons in the solar wind, revealed in the 1970s (e.g., Robbins et al. 1970; Asbridge et al. 1976; Marsch et al. 1982b), have also attracted much attention in the context of plasma kinetic instabilities (e.g., Gary et al. 2000a, 2000b; Li & Habbal 2000; Lu et al. 2006; Verscharen et al. 2013). Effects of the differential flow on proton temperature anisotropy instabilities have been investigated by linear Vlasov–Maxwell theory (Podesta & Gary 2011) and by hybrid simulation (Hellinger & Trávníček 2006; Markovskii et al. 2018). These studies demonstrated that (1) the presence of alpha–proton differential flow contributes to a larger growth rate of the proton cyclotron and parallel firehose instabilities; (2) it can break the symmetry of the unstable waves for their propagation directions so that proton cyclotron (parallel firehose) instability preferentially generates cyclotron (magnetosonic) waves propagating parallel (antiparallel) to the direction of the differential flow vector V_d. In particular, result (2) above was employed to explain the domination of LH polarization of ECWs with the assumption that V_d points outward from the Sun (Podesta & Gary 2011; Zhao et al. 2017b, 2019).

Note that, according to theory (Podesta & Gary 2011), one can deduce that the dominant polarization should be RH polarization once V_d is observed to actually be toward the Sun. However, this deduction, to the best our knowledge, has not been examined by any in situ observation. Moreover, the presence of V_d with a direction toward the Sun is possible, especially for the slow solar wind (e.g., Fu et al. 2018). In this regard, some investigation on the occurrence of ECWs with various directions of V_d should be desirable.

In this paper, we report our finding that the occurrence of ECWs in the solar wind show clear dependence on the radial angle of V_d. In particular, LH ECWs can become secondary

with a percentage much lower than that of RH ECWs when V_d is directed toward the Sun, which should provide a crucial indication for the effect of alpha–proton differential flow. The data and analysis methods used in this paper are described in Section 2. The results are presented in Section 3. Section 4 provides the discussion and conclusion.

2. Data and Analysis Methods

The data used in the present paper are based on the *Wind* mission, which is a comprehensive solar wind laboratory in a halo orbit around the L1 Lagrange point. The magnetic field data are from the Magnetic Field Investigation (MFI) instrument sampled at a cadence of 0.092 s (Lepping et al. 1995), and the plasma data are from the Solar Wind Experiment (SWE) instrument working at a cadence of 92 s (Ogilvie et al. 1995). The plasma data can give the ion (proton and alpha particle) bulk velocity and the perpendicular and parallel temperatures with respect to the background magnetic field; these ion data are produced via a nonlinear-least-squares bi-Maxwellian fit of ion spectrum from the Faraday cup (Kasper et al. 2006). The differential flow vector is defined as $V_d = V_\alpha - V_p$ in this paper, where V_α and V_p are proton and alpha particle bulk velocities, respectively.

It has been acknowledged that the solar wind coming from different source regions on the solar surface often results in different physical situations (e.g., Xu & Borovsky 2015). In order to reduce the possible combined effect of solar winds with different origins, a categorization of the solar wind should be appropriate. A traditional categorization approach is frequently based on the solar wind speed, but studies show that the speed is not necessarily a good parameter for characterization of the solar wind (Marsch et al. 1981; Stakhiv et al. 2015; D'Amicis et al. 2019; Stansby et al. 2019). Instead of the traditional approach, the categorization in this paper is conducted by an eight-dimensional scheme for four-type solar wind categorization based on the machine-learning technique with the k-nearest neighbor classifier (Li et al. 2018). The eight parameters are from, or can be derived from, typical solar wind observations, such as the magnetic field strength, proton density and temperature, solar wind speed, and alpha particle density. The four types of solar winds include coronal-hole-origin (CHO) wind, streamer-belt-origin (SBO) wind, sector-reversal-region (SRR) wind, and ejecta.

The CHO wind refers to the fast solar wind coming from the open field lines in a coronal hole, with a speed generally >500 km s^{-1} at 1 au (Sheeley et al. 1976; Cranmer 2002; McComas et al. 2008; Cranmer 2009). It is characterized typically by a high proton temperature, low plasma density, and outward propagating Alfvén waves (Schwenn 2006). Moreover, this type of wind usually has a relatively steady alpha particle abundance, and the alpha particles often stream faster than protons with a differential velocity comparable to the local Alfvén velocity (Marsch et al. 1982b; Fu et al. 2018). The SBO wind refers to the plasma originating from either the edge of a coronal hole near a streamer belt or the edge of an open streamer, while the SRR wind involves the plasma from the tip of the open streamer where a magnetic sector reversal exists (Gosling et al. 1981; Antonucci et al. 2005; Marsch 2006; Foullon et al. 2009). Both the SBO and SRR winds contribute to the slow solar wind with a speed often $\lesssim 400$ km s^{-1} (Schwenn 2006; Xu & Borovsky 2015). Compared with the CHO wind, they are more variable and filamentary, and have a
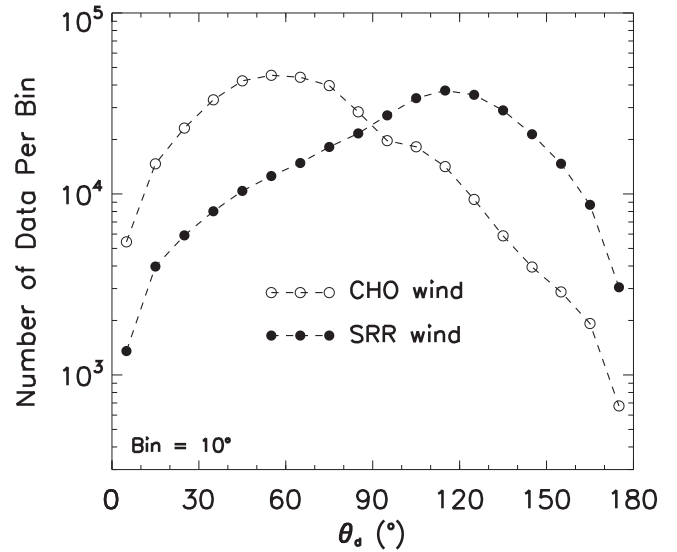

Figure 1. Data distributions regulated by the radial angle θ_d, where open and filled circles represent the CHO and SRR winds, respectively.

low proton temperature, high plasma density, low alpha particle abundance, and small alpha–proton differential velocity (Schwenn 2006; Fu et al. 2018). The ejecta concerns the transient wind denoted as coronal mass ejections that may prevail during the solar maximum (Schwenn 2006; Chen 2011).

One relevant issue is that the types of solar winds are assessed by probabilities in the categorization scheme. Probabilistic approaches to k-nearest neighbor classification have already been proposed by many authors (e.g., Holmes & Adams 2002; Tomasev et al. 2011). The latest scikit-learn package of python can derive a probability for the k-nearest neighbor classifier, and the probability can be given as

$$P_{ij} = \frac{\exp(-d_{ij})}{\sum_k \exp(-d_{ik})}, \tag{1}$$

where d_{ij} is the Euclidean distance between points i and j. The types with probabilities greater than 0.7 are selected to reduce the uncertainties in this paper.

In addition, we discard any observation with $V_d/V_p < 1\%$ since in the case V_d would have a large uncertainty (Kasper et al. 2006; Alterman et al. 2018). Finally, the sample number is about 3.5×10^5 (25%) for the CHO wind, 6.5×10^5 (47%) for the SBO wind, 3.1×10^5 (22%) for the SRR wind, and 8.2×10^4 (6%) for the ejecta during 2005–2015. Note that (1) the ejecta has the smallest sample number, and its physical situation is complicated; (2) the SBO wind has the largest sample number, but it seems to be a transition between the CHO wind and the SRR wind based on our primary test; and (3) the CHO and SRR winds have the comparable sample numbers. Consequently, only solar winds sorted as CHO and SRR winds will be presented to illustrate the main results in the present paper.

Figure 1 plots the data ordered by the radial angle of V_d with a bin of 10°, where open and filled circles represent the CHO and SRR types, respectively. The radial angle is the angle
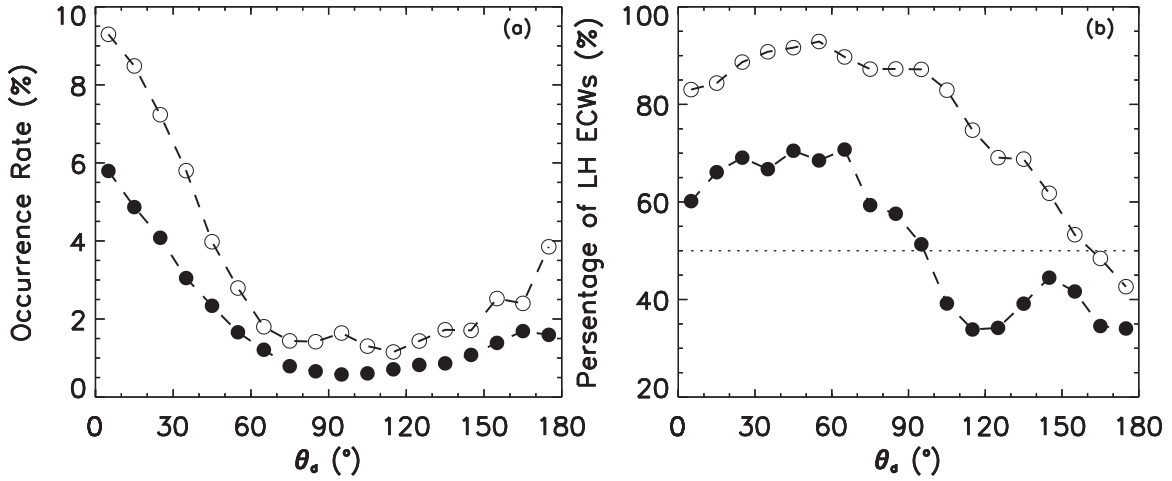
Figure 2. Occurrence rates of ECWs (left panel) and percentages of LH ECWs (right panel) with respect to the radial angle θ_d, where open and filled circles represent the CHO and SRR winds, respectively. The dotted line in the right panel indicates a value of 50%.

between V_d and R (the radial vector of the Sun), defined as

$$\theta_d = \frac{180°}{\pi} \arccos\left(\frac{V_d \cdot R}{|V_d||R|}\right), \quad (2)$$

where arccos refers to the branch of the inverse cosine function with range $[0, \pi]$; an angle $<90°$ means V_d pointing outward from the Sun while an angle $>90°$ denotes it toward the Sun. One can see that there are a considerable number of observations with V_d directed toward the Sun for the CHO wind, and most observations of the SRR wind exhibit V_d toward the Sun.

The survey of ECWs is carried out by an automatic wave detection procedure that was developed by Zhao et al. (2017a, 2018). The procedure mainly consists of three steps. The first step is to calculate the reduced magnetic helicity spectrum in the frequency range from 0.05 to 1 Hz for a given magnetic field interval (e.g., Matthaeus & Goldstein 1982; He et al. 2011). If the spectrum has absolute values $\geqslant 0.7$ in some frequency band (with a minimum bandwidth of 0.05 Hz), the second step will begin with identifying an enhanced power spectrum. The enhancement requires transverse wave power three times larger than the background power in the same frequency band. When the above two steps are fulfilled, the third step follows to record the wave with an amplitude criterion of 0.1 nT; the wave amplitude is obtained with employing a band-pass filter technique (Wilson et al. 2009). Note that the magnetic helicity is described with respect to the direction of the local background magnetic field in the procedure, and a negative (positive) helicity implies LH (RH) polarization. The magnetic field data are first converted into a field-aligned coordinate system with the z direction along the direction of the background magnetic field (i.e., an average field over the period of the interval) before the magnetic helicity is calculated. This operation removes the inversion of the sign of magnetic helicity when the magnetic field direction changes from Sunward to anti-Sunward or vice versa depending on, for instance, the sector structure of the solar wind.

3. Results

The occurrence rate and polarization sense should be two important physical parameters to understand ECWs concerning

their generation mechanism (Zhao et al. 2019). The wave detection procedure described in Section 2 can give the time intervals of ECW occurrence, and therefore allows us to calculate their occurrence rate. The polarization sense of ECWs can also be determined directly by the sign of the spectrum values of magnetic helicity. Figure 2 presents the occurrence rates of ECWs (left panel) and the percentages of LH ECWs (right panel) regulated by the radial angle of V_d, where open and filled circles are for CHO and SRR winds, respectively. The percentages refer to the ratio of the number of time intervals with LH ECWs to the total number of time intervals with either LH or RH ECWs.

Figure 2 shows that the occurrence rates and the percentages of LH ECWs significantly depend on the radial angle θ_d. The occurrence rate for the CHO wind as well as that for the SRR wind decreases from the maximum in the $0°$–$10°$ bin to the minimum at $\theta_d \sim 90°$ and then slightly increases with θ_d. The percentage of LH ECWs with $\theta_d < 90°$ is usually larger than that with $\theta_d > 90°$ for either the CHO wind or the SRR wind. In both cases the percentages generally exceed 50% when $\theta_d < 90°$, and there are enhancements of the percentages at radial angle around $50°$. As θ_d increases from about $90°$ to $180°$, the percentage rapidly reduces from about 87.2% to 42.6% for the CHO wind, and it fluctuates around 40% with a minimum of 33.8% for the SRR wind. This means that LH ECWs can become secondary when V_d is directed toward the Sun, especially in the SRR wind.

In order to understand the implication of results presented in Figure 2, proton temperature anisotropies and parameters for alpha particles are investigated. The temperature anisotropies are described by $T_\perp/T_\parallel$, where $T_\perp$ and $T_\parallel$ are proton temperatures perpendicular and parallel to the background magnetic field, respectively. Figure 3 plots the probability density distributions $p(\theta_d, T_\perp/T_\parallel)$ for the CHO wind (top panel) and the SRR wind (bottom panel), respectively. Here the expression $p = n/(N\Delta\theta_d\Delta R)$ is used, where n and N are the sample number in each cell and the total sample number in each panel, respectively, $\Delta\theta_d\Delta R$ represents the size of the cell with $R = T_\perp/T_\parallel$. One may first find that proton temperature anisotropies are common in solar wind plasmas. This means that ECWs will be excited by the temperature-anisotropy-driven instabilities once their threshold conditions are fulfilled. Note that the distributions of $T_\perp/T_\parallel$ can be different for
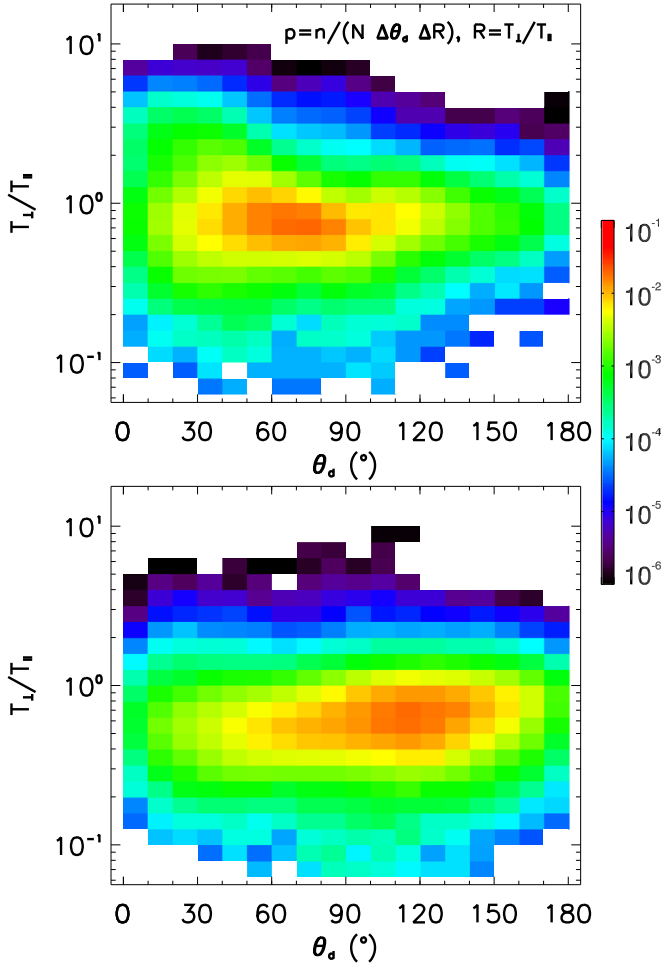
Figure 3. Probability density distributions $p(\theta_d, T_\perp/T_\parallel)$ for the CHO wind (top panel) and the SRR wind (bottom panel), respectively.

different θ_d as well as for different types of solar winds. The plasma of the CHO wind with $\theta_d < 90°$ is characterized by the widest distribution of $T_\perp/T_\parallel$ relative to other plasmas.

The parameters for alpha particles investigated in this study mainly include the density and differential velocity. It has been found that the kinetic energy ratio, defined by

$$\xi_\alpha = \frac{m_\alpha N_\alpha V_d^2}{m_p N_p V_A^2}, \qquad (3)$$

is a relevant parameter to discuss the occurrence of ECWs (Zhao et al. 2019), where m_α and N_α (m_p and N_p) are the mass and number density of alpha particles (protons), and V_A is the local Alfvén velocity. Figure 4 displays medians of ξ_α with respect to θ_d. Several points can be found as follows. First, the median of ξ_α for the CHO wind is always larger than that for the SRR wind in a given radial angle bin. Second, the median of ξ_α in the 0°–10° bin is larger than that in the 170°–180° bin regardless of the solar wind types. Third, there is a distinct maximum with $\theta_d \sim 50°$ for the CHO wind.

The parameter ξ_α may represent the kinetic energy of alpha particle flow in the proton reference frame; it is normalized by the kinetic energy of protons with a bulk velocity V_A for the sake of convenience. Note that usually only the parameter V_d/V_A is investigated in existing literature in which a fixed N_α/N_p is used (e.g., Hellinger & Trávníček 2006; Podesta &
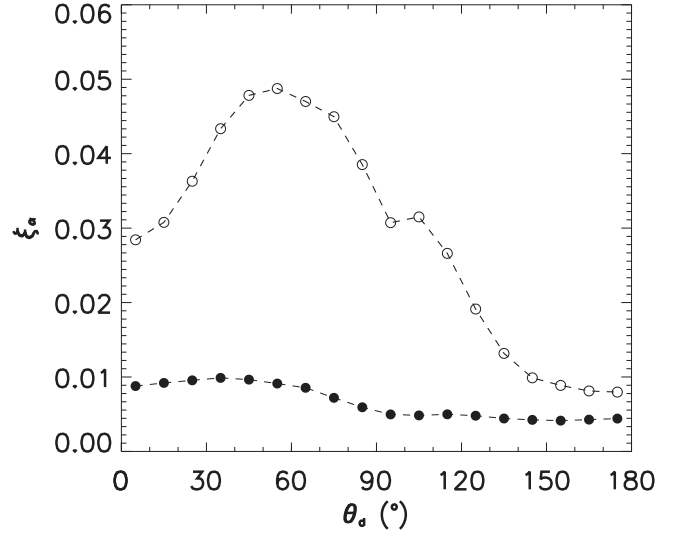

Figure 4. Medians of kinetic energy ξ_α with respect to the radial angle θ_d, where open and filled circles represent the CHO and SRR winds, respectively.

Gary 2011). The proposal of ξ_α in the present paper should be clarified. For this purpose Figure 5 is plotted, where the top panel is for V_d/V_A and the bottom panel is for N_α/N_p with respect to the radial angle θ_d. It is found that the wave occurrence rates shown in Figure 2 cannot be well understood just in terms of V_d/V_A (or just by N_α/N_p). The median of V_d/V_A for SRR wind (filled circles in top panel) is approximately a constant around 0.24, and it is nearly equal to or even exceeds that for CHO wind when $\theta_d > 140°$. Here one may expect that an approximately constant wave occurrence rate should arise irrespective of θ_d for the SRR wind, and comparable occurrence rates between the CHO and SRR winds would happen if $\theta_d > 140°$. However, it is not the case since the occurrence rate for SRR wind is considerably higher when θ_d is small, and on the other hand it is much lower than that for CHO wind when θ_d approaches 180°. This disagreement seems to be removed by the changing N_α/N_p for SRR wind shown in the bottom panel of Figure 5, because the median of N_α/N_p for SRR wind is significantly higher when θ_d is small, and significantly lower than that for CHO wind when θ_d is large. Moreover, it is revealed that large occurrence rates take place mainly at regions with larger V_d/V_A and/or higher N_α/N_p when occurrence rates of ECWs are investigated in the space of (V_d/V_A, N_α/N_p) (Zhao et al. 2019). These results seem to imply that both V_d/V_A and N_α/N_p are simultaneously relevant to the occurrence of the ECWs, which causes us to speculate that an integrated parameter consisting of V_d/V_A and N_α/N_p should be appropriate. Consequently, the kinetic energy ratio ξ_α is proposed to discuss the occurrence of the ECWs. One should keep in mind that this proposal is based on our analyses of observation data since a specific theory concerning ξ_α is absent.

4. Discussion and Conclusion

Two points revealed by Figure 2(a) should be notable. One is that the occurrence rate for the CHO wind is always higher than that for the SRR wind at a fixed radial angle bin. The other is that the occurrence rate in the 0°–10° bin is much higher than that in the 170°–180° bin for either the CHO wind or the SRR wind. We propose here that the temperature-anisotropy-driven
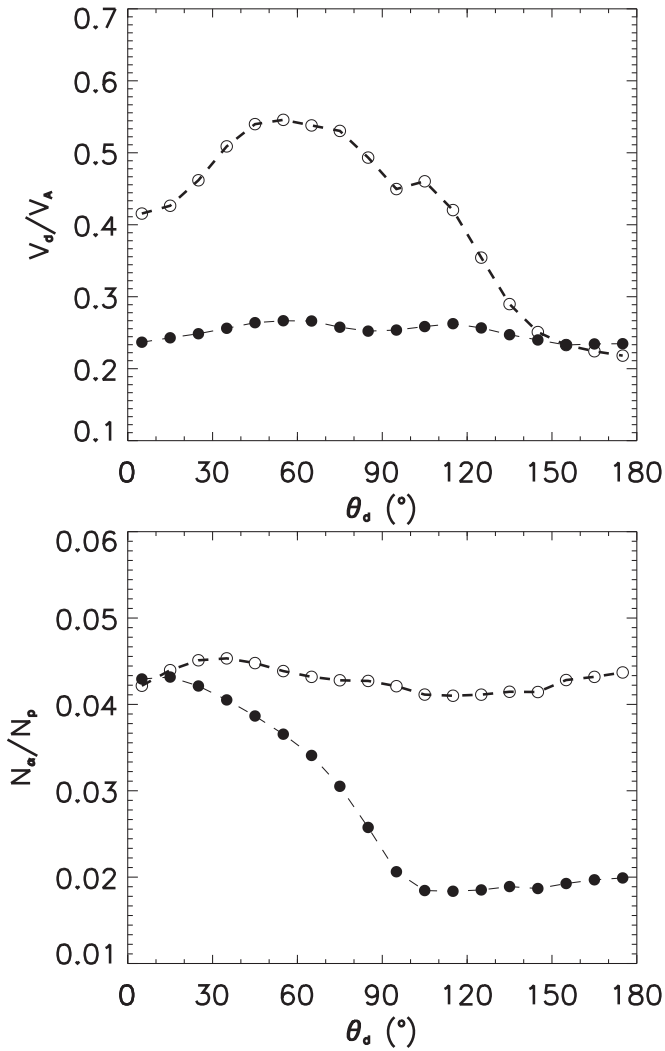
Figure 5. Medians of V_d/V_A (top panel) and N_α/N_p (bottom panel) with respect to the radial angle θ_d, where open and filled circles represent the CHO and SRR winds, respectively.

instabilities with the effect of the alpha–proton differential flow are likely responsible for the generation of ECWs in the solar wind. The presence of alpha–proton differential flow contributes to the excitation of the instabilities; a faster differential flow gives rise to a more rapid growth of the instabilities (Podesta & Gary 2011), and therefore higher occurrence rates of ECWs in observations. Based on this conception, both points in Figure 2(a) can be understood since Figure 4 shows that (1) statistically the kinetic energy (represented by an energy ratio defined by Equation (3)) of the differential flow for the CHO wind is always larger than that for the SRR wind in a given radial angle bin; and (2) the kinetic energy in the 0°–10° bin is also greater than that in the 170°–180° bin for either the CHO wind or the SRR wind.

In the above discussion one may realize that there is still an inconsistency between occurrence rates and kinetic energies when the radial angle approaches 90°. For a given solar wind type the occurrence rate in this region is much lower relative to that in other regions while it is not the case for the kinetic energy. We speculate that this is due to the limit from observation. A lot of ECWs would possibly not be recognized when the radial angle is around 90°. In this region the spacecraft probably crosses approximately perpendicularly to

the wave vector of ECWs and fails to detect the variation of the wave fields. Here we refer to the fact that the differential flow is believed to be aligned with the ambient magnetic field (Kasper et al. 2006; Fu et al. 2018), and meanwhile the ECWs usually propagate nearly parallel to the magnetic field (Jian et al. 2009; Zhao et al. 2018).

The result concerning percentages of LH ECWs in this paper may provide a crucial indication for the effect of alpha–proton differential flow on propagation direction of ECWs. Figure 2(b) shows that the percentages of LH ECWs are significantly different between the case of differential flow with direction outward from the Sun and that with direction toward the Sun, which is consistent with the theory by Podesta & Gary (2011). According to the theory, the alpha–proton differential flow with direction outward from the Sun causes proton cyclotron instability ($T_\perp > T_\parallel$) to preferentially generate cyclotron waves propagating away from the Sun, and it leads parallel firehose instability ($T_\perp < T_\parallel$) to preferentially generate magnetosonic waves propagating toward the Sun. Note that magnetosonic waves are inherently RH waves in the plasma frame, but these waves shall appear as LH waves in the spacecraft frame because their polarization will be reversed in this reference frame by large Doppler shifts due to the fast motion of the solar wind (Jian et al. 2009; Gary et al. 2016). On the other hand, cyclotron waves excited by the proton cyclotron instability tend to propagate toward the Sun while magnetosonic waves produced by the firehose instability will propagate preferentially outward once the differential flow is toward the Sun. Consequently, ECWs generated by these two instabilities will be dominated by LH polarization when the differential flow is directed outward, and they will favor RH polarization when the direction of differential flow is toward the Sun.

In addition, there are considerable enhancements of the percentages at radial angle around 50° (Figure 2(b)), and meanwhile the kinetic energies of the differential flow are larger at the same radial angle. This coincidence should be meaningful and can reinforce the indication for the effect of alpha–proton differential flow since the larger kinetic energies of the differential flow at radial angle around 50° would result in more LH ECWs and therefore larger percentages of LH ECWs. Here, one may also note that the percentage is still higher than 50% even though the radial angle is greater than 90° for the CHO wind. This phenomenon, unfortunately, cannot be understood directly in the present paper. A reason for this might be the presence of proton–proton differential flow in the CHO wind, which could make the polarization complicated in intuition. One notable result is that the percentage of LH ECWs rapidly decreases as the radial angle approaches 180° for the CHO wind. An investigation on the role of proton–proton differential flow is beyond the scope of this paper and is desirable for future study.

Observations of LH ECWs with a percentage less than 50% in the solar wind are rarely reported in previous literature; to the best of our knowledge, only Zhao et al. (2018) reported the percentages less than 50% in 6 months among 84 months based on the *STEREO* mission. This should be because previous surveys did not discriminate the directions of alpha–proton differential flows. In the case in which the dominance of RH ECWs would be hidden by more LH ECWs from the region with the outwardly directed differential flows. The result in Figure 2(b) reveals that a low percentage of LH ECWs can arise for the CHO wind when the radial angle is near 180°, and

it is particularly common for the SRR wind once the radial angle exceeds 90°. In this regard, this paper tends to present a condition for RH ECWs dominating. That is, a plasma with the alpha–proton differential flow directed toward the Sun.

In conclusion, this paper reveals that the occurrence rates and polarization senses of ECWs significantly depend on the direction of alpha–proton differential flow in the solar wind. It is shown that the dominant polarization is LH polarization when the differential flow points outward from the Sun, while it can be RH polarization when the differential flow points in the direction toward the Sun. Further investigation on proton and alpha particles illustrates that large kinetic energies of the differential flow correspond to high occurrence rates of ECWs. These results are well in line with the theory for effects of alpha–proton differential flow on proton temperature anisotropy instabilities.

ORCID iDs

G. Q. Zhao ● https://orcid.org/0000-0002-1831-1451
H. Q. Feng ● https://orcid.org/0000-0003-2632-8066
D. J. Wu ● https://orcid.org/0000-0003-2418-5508

References

Alterman, B. L., Kasper, J. C., Stevens, M. L., & Koval, A. 2018, ApJ, 864, 112
Antonucci, E., Abbo, L., & Dodero, M. A. 2005, A&A, 435, 699
Asbridge, J. R., Bame, S. J., Feldman, W. C., & Montgomery, M. D. 1976, JGR, 81, 2719
Boardsen, S. A., Jian, L. K., Raines, J. L., et al. 2015, JGRA, 120, 10207
Chen, P. F. 2011, LRSP, 8, 1
Cranmer, S. R. 2002, SSRv, 101, 229
Cranmer, S. R. 2009, LRSP, 6, 3
D'Amicis, R., Matteini, L., & Bruno, R. 2019, MNRAS, 483, 4665
Foullon, C., Lavraud, B., Wardle, N. C., et al. 2009, SoPh, 259, 389
Fu, H., Madjarska, M. S., Li, B., Xia, L., & Huang, Z. 2018, MNRAS, 478, 1884
Gary, S. P. 1993, Theory of Space Plasma Microinstabilities (Cambridge: Cambridge Univ. Press), 193
Gary, S. P. 2015, RSPTA, 373, 40149
Gary, S. P., Jian, L. K., Broiles, T. W., et al. 2016, JGRA, 121, 30
Gary, S. P., Montgomery, M. D., Feldman, W. C., & Forslund, D. W. 1976, JGR, 81, 1241
Gary, S. P., Yin, L., Winske, D., & Reisenfeld, D. B. 2000a, JGR, 105, 20
Gary, S. P., Yin, L., Winske, D., & Reisenfeld, D. B. 2000b, GeoRL, 27, 1355

Gosling, J. T., Borrini, G., Asbridge, J. R., et al. 1981, JGR, 86, 5438
He, J., Marsch, E., Tu, C., Yao, S., & Tian, H. 2011, ApJ, 731, 85
He, J., Wang, L., Tu, C., Marsch, E., & Zong, Q. 2015, ApJL, 800, L31
He, J., Zhu, X., Chen, Y., et al. 2018, ApJ, 856, 148
Hellinger, P., & Trávníček, P. 2006, JGRA, 111, A01107
Hellinger, P., Trávníček, P., Kasper, J. C., & Lazarus, A. J. 2006, GeoRL, 33, L09101
Hollweg, J. V. 1975, RvGSP, 13, 263
Holmes, C. C., & Adams, N. M. 2002, Journal of the Royal Statistical Society: Series B (Statistical Methodology), 64, 295
Hu, Y. Q., & Rifai Habbal, S. 1999, JGR, 104, 17045
Jian, L. K., Russell, C. T., Luhmann, J. G., et al. 2009, ApJL, 701, L105
Jian, L. K., Russell, C. T., Luhmann, J. G., et al. 2010, JGRA, 115, A12115
Jian, L. K., Wei, H. Y., Russell, C. T., et al. 2014, ApJ, 786, 123
Kasper, J. C., Lazarus, A. J., & Gary, S. P. 2002, GeoRL, 29, 1839
Kasper, J. C., Lazarus, A. J., Steinberg, J. T., Ogilvie, K. W., & Szabo, A. 2006, JGRA, 111, A03105
Lepping, R. P., Acúña, M. H., Burlaga, L. F., et al. 1995, SSRv, 71, 207
Li, H., Wang, C., Tu, C., & Xu, F. 2018, E&SS, submitted
Li, Q. H., Yang, L., Wu, D. J., & Wang, T. Y. 2019, ApJ, 874, 55
Li, X., & Habbal, S. R. 2000, JGR, 105, 7483
Lu, Q. M., Xia, L. D., & Wang, S. 2006, JGRA, 111, A09101
Markovskii, S. A., Chandran, B. D. G., & Vasquez, B. J. 2018, ApJ, 856, 153
Marsch, E. 2006, LRSP, 3, 1
Marsch, E., Ao, X.-Z., & Tu, C.-Y. 2004, JGRA, 109, A04102
Marsch, E., Goertz, C. K., & Richter, K. 1982a, JGR, 87, 5030
Marsch, E., Rosenbauer, H., Schwenn, R., Muehlhaeuser, K.-H., & Denskat, K. U. 1981, JGR, 86, 9199
Marsch, E., Rosenbauer, H., Schwenn, R., Muehlhaeuser, K.-H., & Neubauer, F. M. 1982b, JGR, 87, 35
Matthaeus, W. H., & Goldstein, M. L. 1982, JGR, 87, 6011
McComas, D. J., Ebert, R. W., Elliott, H. A., et al. 2008, GeoRL, 35, L18103
Ogilvie, K. W., Chornay, D. J., Fritzenreiter, R. J., et al. 1995, SSRv, 71, 55
Omidi, N., Isenberg, P., Russell, C. T., Jian, L. K., & Wei, H. Y. 2014, JGRA, 119, 1442
Podesta, J. J., & Gary, S. P. 2011, ApJ, 742, 41
Robbins, D. E., Hundhausen, A. J., & Bame, S. J. 1970, JGR, 75, 1178
Rodríguez-Martínez, M., Blanco-Cano, X., Russell, C. T., et al. 2010, JGRA, 115, A09207
Russell, C., & Blancocano, X. 2007, JASTP, 69, 1723
Schwartz, S. J., Burgess, D., & Moses, J. J. 1996, AnGeo, 14, 1134
Schwenn, R. 2006, SSRv, 124, 51
Sheeley, N. R., Jr., Harvey, J. W., & Feldman, W. C. 1976, SoPh, 49, 271
Smith, C. W., Goldstein, M. L., Gary, S. P., & Russell, C. T. 1985, JGR, 90, 1429
Soucek, J., Escoubet, C. P., & Grison, B. 2015, JGRA, 120, 2838
Stakhiv, M., Landi, E., Lepri, S. T., Oran, R., & Zurbuchen, T. H. 2015, ApJ, 801, 100
Stansby, D., Horbury, T. S., & Matteini, L. 2019, MNRAS, 482, 1706
Tomasev, N., Radovanović, M., Mladenić, D., & Ivanović, M. 2011, in Proc. ACM Conf. 20, Information and Knowledge Management, CIKM'11 (New York: ACM)
Verscharen, D., Bourouaine, S., & Chandran, B. D. G. 2013, ApJ, 773, 163
Wilson, L. B., III, Cattell, C. A., Kellogg, P. J., et al. 2009, JGRA, 114, A10106
Wong, H. K., Goldstein, M. L., & Smith, C. W. 1991, JGR, 96, 285
Woodham, L. D., Wicks, R. T., Verscharen, D., & Owen, C. J. 2018, ApJ, 856, 49
Xiang, L., Wu, D. J., & Chen, L. 2018a, ApJ, 869, 64
Xiang, L., Wu, D. J., & Chen, L. 2018b, ApJ, 857, 108
Xu, F., & Borovsky, J. E. 2015, JGRA, 120, 70
Yoon, P. H. 2017, RvMPP, 1, 4
Zhao, G. Q., Chu, Y. H., Lin, P. H., et al. 2017a, JGRA, 122, 4879
Zhao, G. Q., Feng, H. Q., Wu, D. J., et al. 2018, JGRA, 123, 1715
Zhao, G. Q., Feng, H. Q., Wu, D. J., Chu, Y. H., & Huang, J. 2017b, ApJL, 847, L8
Zhao, G. Q., Feng, H. Q., Wu, D. J., Pi, G., & Huang, J. 2019, ApJ, 871, 175